DEUTSCHES ELEKTRONEN-SYNCHROTRON DESY

DESY 85-052
June 1985

PHYSICS AT HERA

by

G. Wolf

Stanford Linear Accelerator Center, Stanford University

and

Deutsches Elektronen-Synchrotron DESY, Hamburg

ISSN 0418-9833

NOTKESTRASSE 85 · 2 HAMBURG 52

To be sure that your preprints are promptly included in the
HIGH ENERGY PHYSICS INDEX ,
send them to the following address (if possible by air mail) :

DESY
Bibliothek
Notkestrasse 85
2 Hamburg 52
Germany

DESY 85-052
June 1985

ISSN 0418-9833

PHYSICS AT HERA*

GÜNTER WOLF

Stanford Linear Accelerator Center, (SLAC)
Stanford University, Stanford, California 94305

Deutsches Elektronen Synchrotron, (DESY)
Notkestrasse 85, D-2000 Hamburg 52, Germany

1. The HERA Collider

DESY is presently constructing a new storage ring that will provide collisions between 30 GeV electrons and 820 GeV protons. This collider is called HERA which stands for Hadron – Elektron – Ring – Anlage. The layout of the machine is sketched in Fig. 1. HERA intersects the PETRA storage ring which will serve as the injector for electrons and protons. The salient machine parameters are listed in Table 1.

An important aspect of HERA is the polarization of the electron beam. By the emission of synchrotron radiation the circulating electrons become polarized perpendicular to the plane of the ring. From the physics point of view this direction of polarization is not very attractive. What is needed are electrons of a given helicity. The electron spin will be rotated into the longitudinal direction by a spin rotator in front of each interaction region. The spin rotation is undone by a mirror symmetric spin rotator following the interaction region. The degree of longitudinal polarization is expected to be 85%.

The construction schedule is given in Table 2. Ground breaking took place in May 1984. The tunnel should be ready by the end of 1987. The installation of the machine components follows the tunnel boring machine so that by March 1988 the electron ring should be complete. Technically the most demanding components are likely to be the superconducting magnets for the proton ring and the associated cryogenics. Series production of the proton magnets is expected to take from July 1986 until October 1988. The proton ring should be completed by summer 1989. The first ep collisions are foreseen for the beginning of 1990.

* Invited talk given at the 1985 Aspen Winter Physics Conference

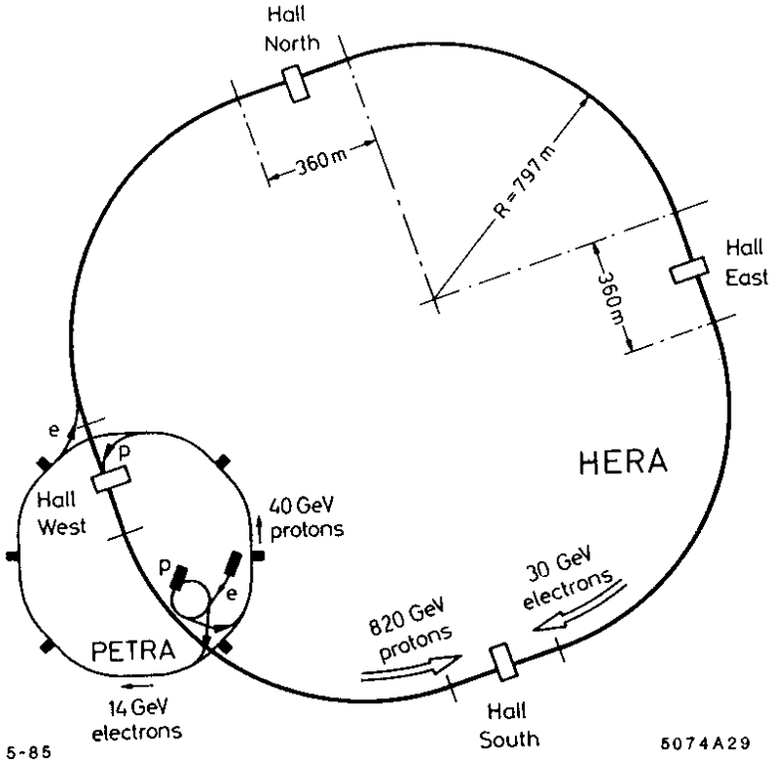

Figure 1. Schematic view of the HERA ring and the preaccelerators (two linear accelerators, two synchrotrons of 100 m diameter, PETRA storage ring). The proton ring is mounted on top of the electron ring.

Table 1. Parameters of HERA

	p-ring		e-ring	units
Nominal energy	820		30	GeV
c.m. energy		314		GeV
Q^2max		98.400		GeV^2
Luminosity		$2.5 \cdot 10^{31}$		cm^{2}s^{-1}
Polarization time			25	min
Number of interaction points		4		
Crossing angle		0		
Free space for experiments		± 5.5		m
Circumference		6336		m
Length of straight sections		360		m
Bending radius	603.8		540.9	m
Magnetic field	4.73		0.1849	T
Energy range	300-820		10-33	GeV
Injection energy	40		14	GeV
Circulating current	130		58	mA
Total number of particles	$2.2 \cdot 10^{13}$		$0.76 \cdot 10^{13}$	
Number of bunches		200		
Number of bunch buckets		220		
Time between crossings		95		nsec
Emittance (ϵ_x/ϵ_y)	0.47/0.24		1.6/0.16	10^{-8}m
Beta function (β_x^*/β_y^*)	10/1.0		2/0.7	m
Beam tune shift (Q_x, Q_y)	0.0026/0.0014		0.023/0.026	
Beam size at crossing σ_x^*	0.12 (0.43)		0.22	mm
Beam size at crossing σ_y^*	0.027		0.013	mm
Beam size at crossing σ_z^*	10		0.9	cm
Energy loss /turn	$1.4 \cdot 10^{-10}$		142.3	MeV
Critical energy	10^{-6}		111	KeV
Max. circumf. voltage	0.7/2		165	MV
Total RF power	1		13.2	MW
RF frequency	52.033/208.13		499.667	MHz
Filling time	20		15	min
Heat loss at 4.2^0K	13.2			kW
Available refrigeration power at 4.2^0K	19.5 kW + 60 g/s			
available refrigeration power at 40^0K	60			kW
cooldown time for one octant	30			hrs

Table 2. The HERA Construction Schedule

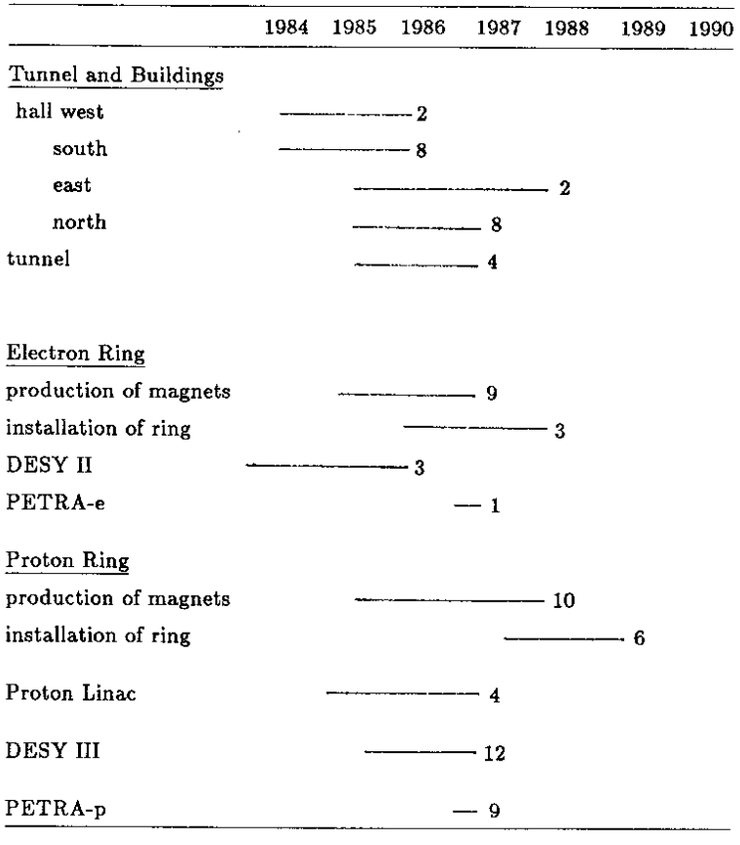

The total cost for HERA is estimated at 654 MDM using 1981 prices. Of this sum 261 MDM are required for sites, buildings and power installations, 112 MDM for the electron ring and 281 MDM for the proton ring. The costs will be born by the German federal government and the city of Hamburg (in the ratio 9:1) and by contributions from Canada, France, Holland, Israel, Italy, and England.

With respect to experiments the planning is as follows. A call has been issued for letters of intent by June 1985. After decisions on the proposed experiments by the end of 1985, the experimenters will have four years for the construction and installation of the detector.

2. HERA Physics: General Considerations

The large momentum transfers possible between electron and proton, $Q^2_{\max} = 10^5$ GeV^2, make HERA first and foremost an electron quark collider. The relevant diagram is shown in Fig. 2. The incoming electron emits a lepton ℓ and exchanges a current j with one of the quarks of the incoming proton. This leads to the emission of a quark q' (= current quark). Depending on whether a neutral current (γ, Z^0) or a charged current (W^-) is exchanged the final state lepton is either an electron or a neutrino (Fig. 3.).

Of course, the scattering process is not confined to the known currents, quarks and leptons. New currents may contribute and new quarks and leptons with masses up to the kinematic limit of 314 GeV may be produced. Any constituents that carry electromagnetic or weak charge and are within the kinematic limits can be produced at HERA. Thus HERA is a hunting ground for the legions of new particles that have been proposed: excited leptons and quarks, lepto quarks, supersymmetric particles, and many more.

Next to electron quark scattering, photon gluon fusion will play an important role at HERA. Photon gluon fusion, depicted in Fig. 4, is presumably the dominant process for the production of heavy quarks $Q = c, b, t, \ldots$

The following discussion of the physics potential that HERA offers is by no

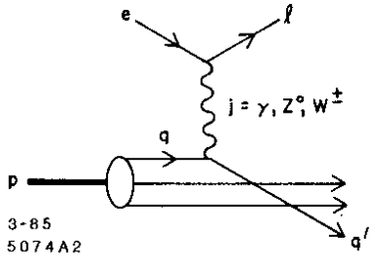

Figure 2. Lepton proton scattering.

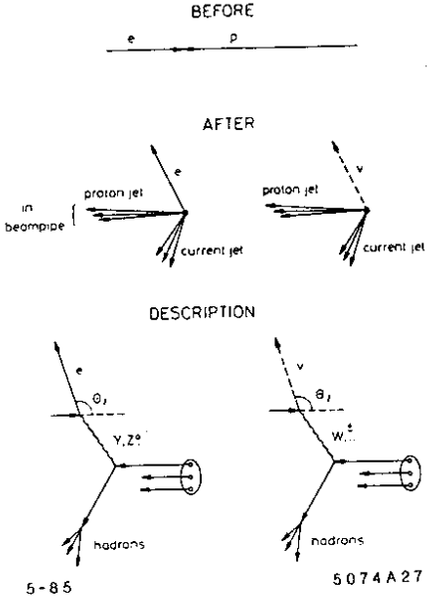

Figure 3. Diagrams for neutral (a) and charged current (b) scattering.

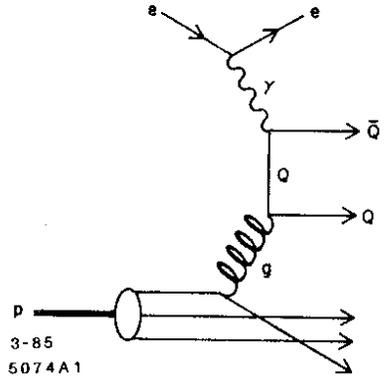

Figure 4. Quark pair production by photon gluon fusion.

means exhaustive. Rather, a few processes that are archetypical for the different classes of physics will be considered. More detailed studies can be found in Ref. 2, in the 1979 ECFA study report, in the HERA proposal, and in the proceedings of the HERA meetings at Wuppertal, Amsterdam and Genova[3] and in the papers cited there.

3. Electron Scattering And The Proton Structure Functions

3.1 Neutral Current Processes

The diagram that describes ep scattering in lowest order is shown in Fig. 2 (taking $j = \gamma$). The final state partons (quarks, gluons) and the "spectator" remnants from the incident proton are assumed to develop into jets of hadrons. Apart from the total center – of – mass energy squared,

$$s = (p_p + p_e)^2 = m_e^2 + m_p^2 + 2(E_e E_p + p_e p_p) \approx 4 E_e E_p$$

E_e, E_p energies of electron and proton

there are two kinematic variables that describe the inclusive scattering process:

$q^2 = (p_e - p_e')^2 = -Q^2$		square of the four momentum transfer
$W^2 = (q + p_p)^2$		square of the total mass of the final hadronic system.

or equivalently

$x = \frac{Q^2}{2(q \cdot p_p)} = \frac{Q^2}{2m_p \nu}$		the Bjorken scaling variable.
$y = \frac{(q \cdot p_p)}{(q \cdot p_e)} = \frac{\nu}{\nu_{\max}}$,		note that $Q^2 \simeq sxy$.

In the rest system of the incoming proton ν measures the energy transferred by the current. The maximum value which ν can reach is

$$\nu_{\max} = \frac{s - (m_e + m_p)^2}{2m_p} \approx \frac{s}{2m_p} = 2E_e E_p / m_p$$

For $E_e = 30$ GeV, $E_p = 820$ GeV : $\nu_{\max} = 52$ TeV. HERA therefore is equivalent to a fixed target experiment with an incident lepton beam of 52 TeV.

The one photon exchange cross section can be written in terms of two dimensionless structure functions F_1, F_2 which are functions of ν, Q^2 or x, y:

$$\frac{d^2\sigma(\gamma)}{dxdy} = \frac{4\pi\ \alpha^2}{s\ x^2y^2}\ [(1-y)\ F_2\,(x,Q^2)\ +\ xy^2\ F_1(x,Q^2)]$$

In the approximation that scattering on spin 1/2 partons dominates F_1 can be expressed in terms of F_2 using the Callan - Gross relation : $2x\,F_1 = F_2$.

This leads to

$$\frac{d^2\sigma(\gamma)}{dx\,dy} \approx \frac{4\pi\,\alpha^2}{s\,x^2y^2}\left(1-y+\frac{y^2}{2}\right)\ F_2\ (x,Q^2)$$

In the quark picture, ep scattering is described as incoherent eq scattering with x measuring the fractional momentum of the struck quark. The structure functions can then be expressed in terms of the quark distribution functions $u(x)$, $d(x)$,...* where $u, d, \ldots$ give the number of $u, d, \ldots$ quarks with fractional momentum between x and $x + dx$:

$$F_2\,(x) = 2xF_1(x) = x[q(x) + \bar{q}(x)]$$

where for the electromagnetic current

$$q(x) = \frac{4}{9}u(x) + \frac{1}{9}d(x) + \frac{1}{9}s(x) + \frac{4}{9}c(x) \quad .$$

At Q^2 values above 10^4 GeV^2 the contribution from Z^0 exchange becomes comparable to that from photon exchange. Formally, the cross section can be written as before,

$$\frac{d^2\sigma(\gamma+Z^0)}{dxdy} = \frac{4\pi\ \alpha^2}{s\ x^2y^2}\ [(1-y)\ F_2\,(x,Q^2)\ +\ y^2x\,F_1(x,Q^2)]$$

where now the structure functions F_1 and F_2 receive contributions from γ exchange, from Z^0 exchange and from the interference between the two processes. In terms of the quarks distribution functions the cross section reads for left (right) handed electrons:[4)]

* The quark distribution functions as well as the structure functions depend on x *and* Q^2. For ease of writing the Q^2 dependence is not shown.

$$\frac{d^2\sigma}{dxdy}\,(e^-\left\{\begin{matrix}L\\R\end{matrix}\right\} + p \to e^-\left\{\begin{matrix}L\\R\end{matrix}\right\} X) =$$

$$\frac{4\pi\alpha^2}{s(xy)^2}\,[Q_u^2\,(u(x)+\bar{u}(x)) + Q_d^2\,(d(x)+\bar{d}(x))]\,x\,(1-y+y^2/2)$$

$$+\ \frac{\alpha}{xy}\,\frac{\sqrt{2}\,G_F\,M_Z^2}{sxy+M_Z^2}\left\{\begin{matrix}1-2\sin^2\vartheta_W\\ -2\sin^2\vartheta_W\end{matrix}\right\}\ \cdot$$

$$\cdot\ \{\ [Q_u(1-4\,Q_u\sin^2\vartheta_W)\,(u(x)+\bar{u}(x))$$

$$-\ Q_d(1+4\,Q_d\sin^2\vartheta_W)(d(x)+\bar{d}(x))]\cdot(1-y+y^2/2)\ \}+$$

$$+\ \frac{\alpha}{xy}\,\frac{\sqrt{2}\,G_F\,M_Z^2}{sxy+M_Z^2}\left\{\begin{matrix}1-2\sin^2\vartheta_W\\ 2\sin^2\vartheta_W\end{matrix}\right\}\ \cdot$$

$$\cdot\ [Q_u\,(u(x)-\bar{u}(x)) - Q_d(d(x)-\bar{d}(x))]\,xy\,(1-y/2)+$$

$$+\ \frac{s}{4\pi}\,\frac{G_F^2\,M_Z^4}{(sxy+M_Z^2)^2}\left\{\begin{matrix}(1-2\sin^2\vartheta_W)^2\\ 4\sin^4\vartheta_W\end{matrix}\right\}\ \cdot$$

$$\cdot\ \{\ [(1-4\,Q_u\sin^2\vartheta_W\ +\ 8\,Q_u^2\sin^4\vartheta_W)\,(u(x)+\bar{u}(x))+$$

$$+\ (1+4\,Q_d\sin^2\vartheta_W\ +\ 8\,Q_d^2\sin^4\vartheta_W)\,(d(x)+\bar{d}(x))]\ .\ (1-y+y^2/2)\ \}\ +$$

$$+\ \frac{s}{4\pi}\,\frac{G_F^2\,M_Z^4}{(sxy+M_Z^2)^2}\left\{\begin{matrix}(1-2\sin^2\vartheta_W)^2\\ -4\sin^4\vartheta_W\end{matrix}\right\}\ \cdot$$

$$\cdot\ \{\ [(1-4\,Q_u\sin^2\vartheta_W)\,(u(x)-\bar{u}(x))+$$

$$+\ (1+4\,Q_d\sin^2\vartheta_W)(d(x)-\bar{d}(x))]\,xy\,(1-y/2)\ \}$$

with $Q_u = 2/3$ and $Q_d = -1/3$.

G_F is the fermi coupling constant, $G_F = \frac{1.02 \cdot 10^{-5}}{M_p^2}$. To simplify the writing, only the $u, \bar{u}$ and $d, \bar{d}$ contributions are shown. The expected event rates have been calculated in Ref. 4 using the structure functions of Ref. 5 and assuming 10,000 h of data taking ($\sim$ 2 years of operation) at an average luminosity of 0.5 $10^{31}\ cm^{-2}s^{-1}$. The results are shown in Fig. 5. Note that Q^2 values less than 3 GeV^2 have been suppressed. There are $20 \cdot 10^6$ events with Q^2 values between 3 and 10^4 GeV^2. Roughly a thousand events have Q^2 values above 10^4 GeV^2 where Z^0 effects dominate. If we demand a minimum of a hundred events we see that neutral currents can be studied with sufficient statistics up to Q^2 values of $3 \cdot 10^4$ GeV^2. The dark corner with $Q^2 < 200$ GeV^2, $y < 0.004$ marks the kinematical region that has so far been explored experimentally. HERA will extend the kinematic region by two orders of magnitude in either variable.

3.2 Charged Current Processes

Charged current reactions, $e^- p \rightarrow \nu X$, proceed through W^- exchange. The cross section for left handed electrons can be written in terms of three structure functions F_1, F_2 and F_3:

$$\frac{d^2\sigma}{dxdy}(e_L^- p \rightarrow \nu X) = \frac{G_F^2 s}{\pi} \frac{1}{(1+Q^2/M_W^2)^2}$$

$$\left[(1-y)\,F_2(x,Q^2) + y^2 x\,F_1(x,Q^2) + \left(y - \frac{y^2}{2}\right) x\,F_3(x,Q^2)\right]$$

The cross section for right handed electrons vanishes since the neutrino is left handed.

$$\frac{d^2\sigma}{dxdy}(e_R^- + p \rightarrow \nu + X) = 0$$

The quark - parton expression for the structure functions is:

$$F_2(x) = 2xF_1(x) = x[q(x) + \bar{q}(x)]$$

$$xF_3(x) = x[q(x) - \bar{q}(x)]$$

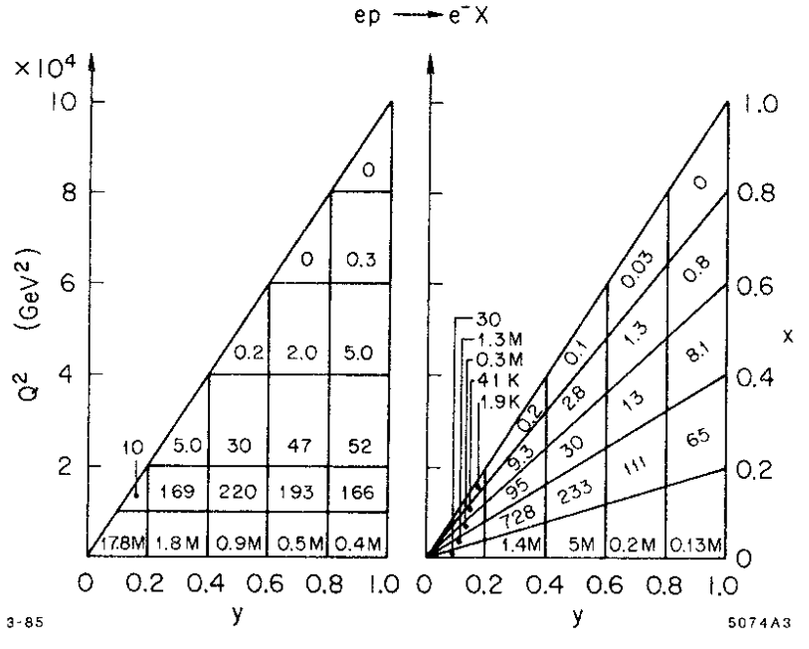

Fig. 5 Expected neutral current event rates for $e^- p \rightarrow e^- X$ from $\gamma + Z^0$ exchange for a luminosity of 200 pb^{-1}.

where

$$q(x) = u(x) + c(x) + \ ...$$

$$\bar{q}(x) = \bar{d}(x) + \bar{s}(x) + \ ...$$

This leads to

$$\frac{d^2\sigma}{dxdy}(e_L^- p \to \nu + X) = \frac{G_F^2 s}{\pi} \frac{1}{(1 + Q^2/M_W^2)^2} x \{ u(x) + (1-y)^2 \bar{d}(x) \}$$

where the higher mass quarks have been omitted. The expected event rates are shown in Fig. 6. They have been calculated[4] under the same assumptions on luminosity and running time as above. Roughly 22,000 events are produced at $Q^2 < 10^4$ GeV^2 and 1700 events at $Q^2 > 10^4$ GeV^2. Figure 6 shows that charged currents can also be studied with sufficient statistics up to $\sim 4 \cdot 10^4$ GeV^2.

The topology of neutral and charged current events is illustrated in Fig. 7. The lepton and the current jet (several jets if gluons are also emitted) emerge on opposite sides of the beam axis; they balance each other in transverse momentum. The debris of the proton are emitted in a very narrow cone (of order 10 mrad) around the proton beam direction which renders their detection difficult. Figures 8 and 9 show neutral and charged current events. In the latter case only the current jet is observable and Q^2, x have to be determined solely from the current jet properties.

A precise determination of the structure functions will open the way to address several fundamental questions:

3.3.1 QCD

The large Q^2 range accessible at HERA will allow a stringent test of QCD which predicts logarithmically falling structure functions. Mass corrections and higher twist contributions which affect present experiments should be negligible at HERA.

The accuracy with which one can hope to measure the QCD scale parameter is around ± 40 MeV for $\Lambda_{QCD} = 200$ MeV.

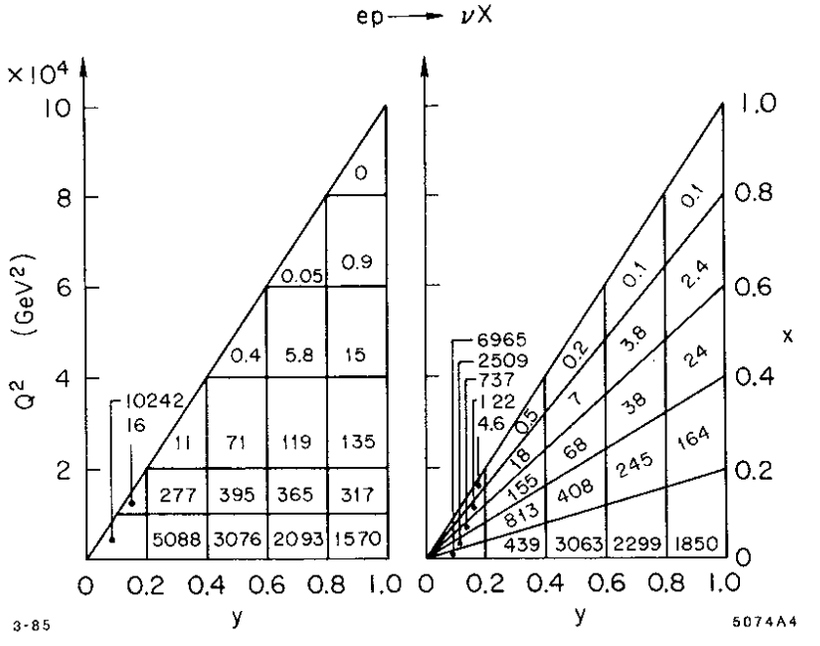

Figure 6. Expected charged current event rates for $e_L^- p \to \nu X$ for a luminosity of 200 pb^{-1}.

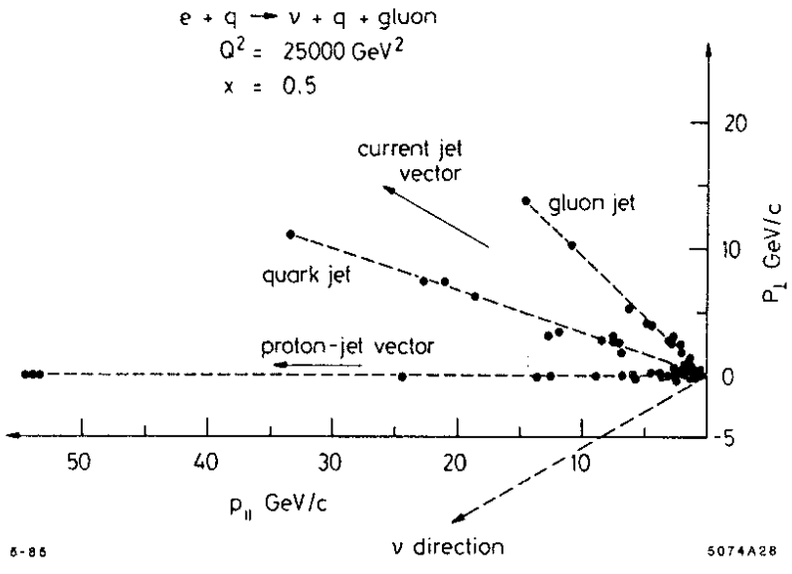

Figure 7. Topology of neutral and charged current events.

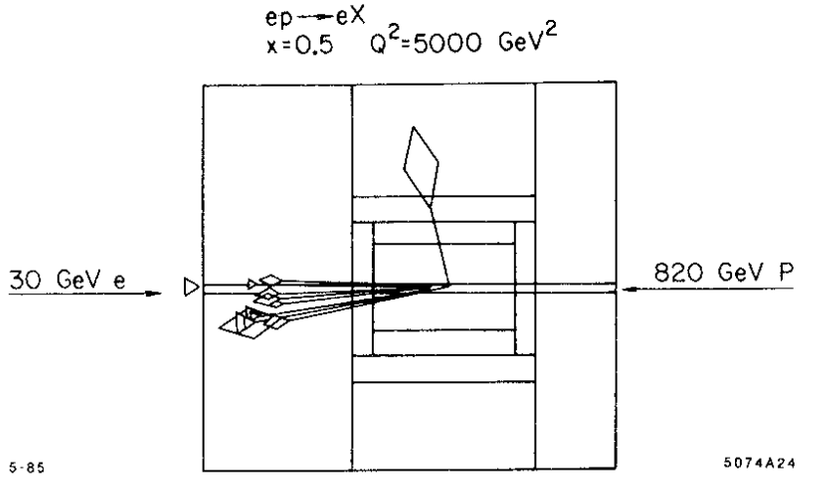

Figure 8. Example of a neutral event.

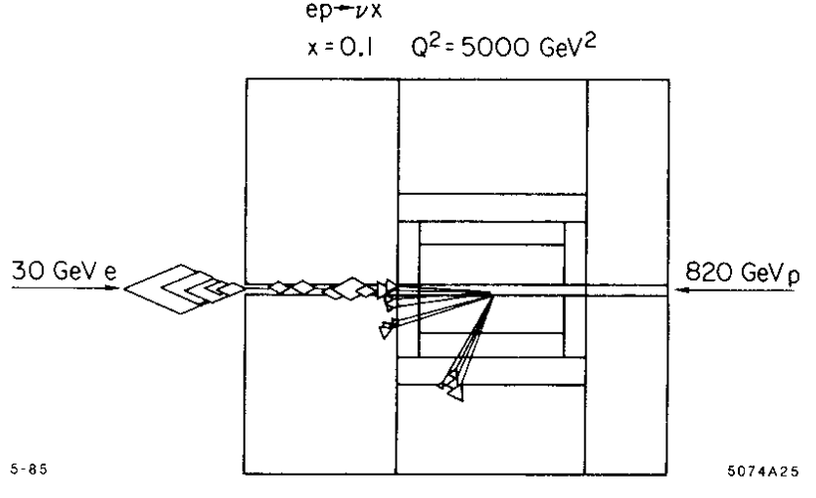

Figure 9. Example of a charged current event.

The same data will also yield accurate measurements for the quark and gluon distribution functions.

3.3.2 *Structure Of Quarks And Electrons*

If quarks and/or electrons are extended objects the structure functions will show power law type deviations from their QCD predicted values. The sensitivity to possible structure of quarks and electrons has been estimated with the help of a model [6] which assumes quarks and electrons to be composites and to have common constituents. The interchange of the constituents leads to a contact term of the form

$$\mathcal{L} \sim \frac{g^2}{\Lambda^2} \sum \bar{e}_\alpha \gamma^\mu e_\alpha \bar{q}_\beta \gamma_\mu q_\beta$$

where α, β denote states of a definite helicity, $\alpha = L, R$; $\beta = L, R$. The mass parameter Λ sets the compositness scale; g measures the coupling strength. For the following $g^2/4\pi = 1$ will be assumed. Figure 10 shows the ratio of the structure functions F_2 obtained *with* the contributions from $\gamma + Z^0$ exchange and the contact interaction, and for γ exchange *alone*:

$$F_2(\gamma + Z^0 + C.I.)/F_2(\gamma)$$

The ratio is shown as a function of Q^2 and x for different Λ values. At Q^2 values above 10^4 GeV^2 a contact interaction with $\Lambda = 1$ TeV leads to large deviations – factors of 5 to 10 — from the standard result. Given two years of data taking HERA will be sensitive up to Λ values of ~ 7 TeV corresponding to distances of $3 \cdot 10^{-18}$ cm. The present lower limits on Λ are 2-4 TeV on e, μ from $e^+e^- \to \mu^+\mu^-$ and 300 GeV for quarks from the total cross section for e^+e^- annihilation into hadrons.[7] A theoretical analysis of some composite models has indicated that the energy of HERA would still be insufficient to see structure in the quarks and electrons[8]. It suggests a lower as well as an upper limit on Λ:

$$\lambda(20 - 30)\text{TeV} \; < \; \Lambda \; < \; 250 \text{ TeV}$$

The lower limit is deduced from the limit on the decay $K^+ \to \pi^+ \mu e$; λ is a number

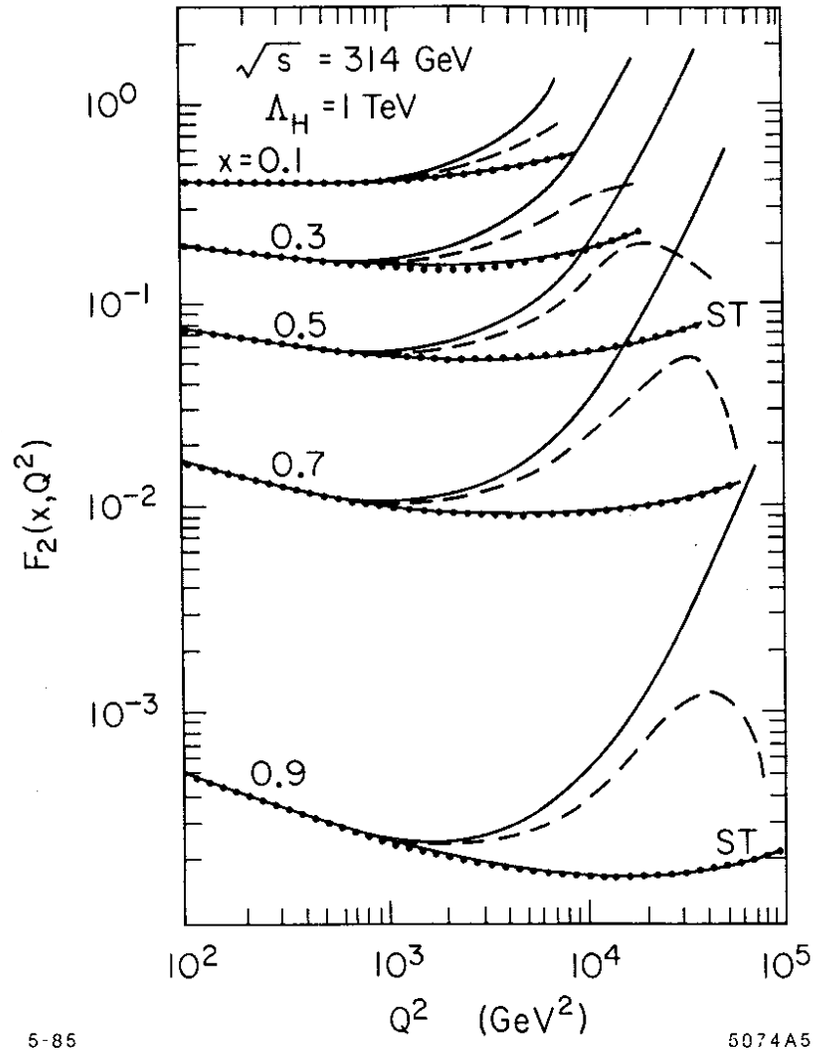

Figure 10. The ratio $F_2(\gamma + Z^0 + C.I)/F_2(\gamma)$.

of order unity. The upper limit stems from cosmological considerations.

3.3.3 New Currents

Altarelli *et al.*, [3] have estimated the effect of a second W_2 on the rate of charged current events. The amplitude for the exchange of the standard $W(W_1)$ can be written as

$$A(Q^2) \sim \frac{g^2}{8(Q^2+m_N^2)} \sim \frac{G_F/\sqrt{2}}{1+Q^2/m_W^2} \; .$$

Under the assumption that the second W couples in the same way to leptons and quarks the amplitude can be written as

$$A_{1+2}(Q^2) \sim \frac{g_1^2}{8(Q^2+m_1^2)} + \frac{g_2^2}{8(Q^2+m_2^2)} \; .$$

The coupling constants g_1, g_2 have to be chosen such that the low Q^2 region remains unchanged, *i.e.*

$$A(0) \equiv \frac{G_F}{\sqrt{2}} = A_{1+2}(0) = \frac{g_1^2}{8m_1^2} + \frac{g_2^2}{8m_2^2} \equiv \frac{g^2}{8m_W^2}$$

taking $m_1 = m_W$ and defining $r = g_2^2/g^2$ the ratio of the cross sections for two W's over one W is given by

$$\frac{\sigma(W_1+W_2)}{\sigma(W_1)} = \left[1 - r\frac{m_1^2}{m_2^2} + r\,\frac{m_1^2}{m_2^2}\,\frac{1+Q^2/m_1^2}{1+Q^2/m_2^2}\right]$$

The ratio is shown in Fig. 11 for different W_2 masses assuming $r = 1$. For m_2 around 200 GeV large deviations from the standard theory result will be observed. The derivations become smaller as m_2 increases. With two years of data taking one will be sensitive to W_2 masses up to $\sim$ 800 GeV.

A similar result holds for neutral currents and additional Z^0's.

3.3.4 Right Handed Currents

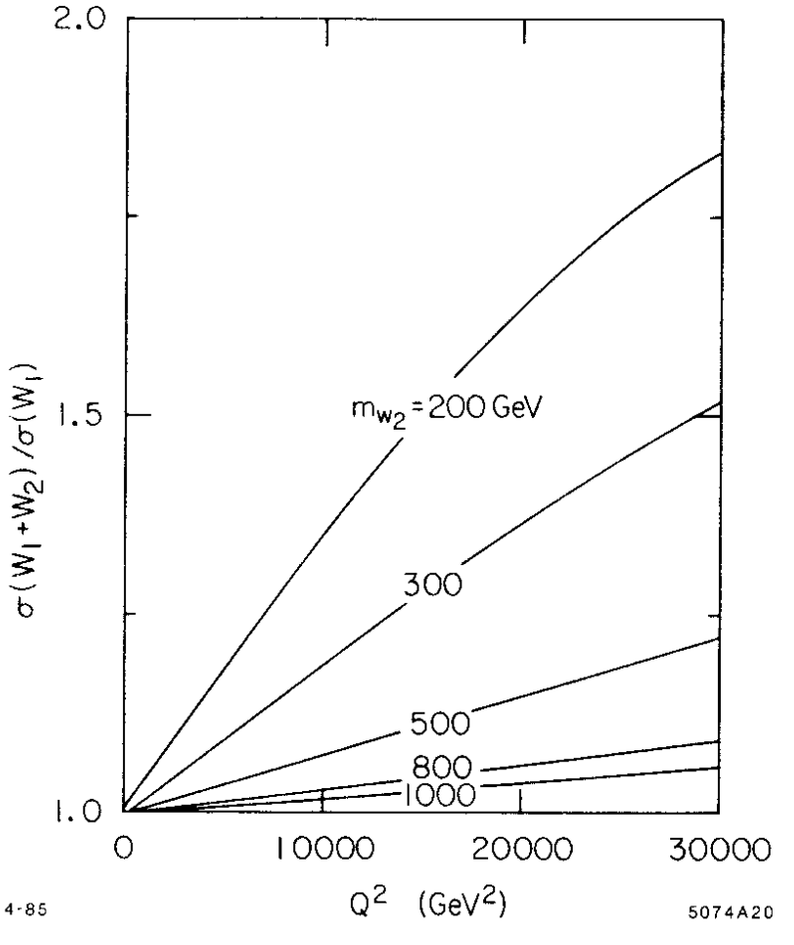

Figure 11. The ratio of the cross sections for two and one W.

One of the great mysteries of weak interactions is the asymmetry between left and right handedness; there are left handed neutrinos and left handed currents and no right handed counter parts. It has long been speculated that left-right symmetry is restored at some higher energy; namely there exist heavy right handed neutrinos N_R that couple to a right handed W_R.[9] The mass of N_R has been related to the masses of the corresponding charged lepton, m_e, and the left handed neutrino m_ν:[10] $m_{N_R} \approx m_e^2/m_\nu$. For electrons this leads to the following prediction for m_{N_R}:

m_ν (eV)	0.1	1	10
m_{N_R} (GeV)	2611	261	26

Several experimental and theoretical limits have been put on the mass of W_R (see Ref. 11):

β decay of μ's	
if ν is a Dirac spinor:	$M_R > 380$ GeV
if ν is a Majorana spinor:	no limit
Nonleptonic decays	$M_R > 200 - 300$ GeV
$K_s^0 - K_L^0$ mass difference	
if the $(K-M)$ matrix elements are the same for W_L and W_R:	$M_R \geq 1 - 2$ TeV
otherwise	no limit

The lower limit on a right handed Z^0 is $M_{Z_R} \geq 150 - 200$ GeV, provided $\sin^2 \vartheta_W < 0.25$.

3.3.5 Search For Right-Handed Currents With Longitudinally Polarized Electrons

Longitudinally polarized electrons make HERA ideally suited to search for right handed currents. Any nonzero cross section contribution to $e_R^- p \to \nu X$ or $e_L^+ p \to \bar{\nu} X$ scattering signals the presence of a right handed charged current (see Sect. 3.2.). In the absence of a W_R contribution:

$$\frac{d^2\sigma}{dxdy}\begin{pmatrix} e_L^- p \\ e_R^+ p \\ e_R^- p \\ e_L^+ p \end{pmatrix} = \frac{G_F^2 s}{\pi} \frac{x}{(1+Q^2/M_W^2)^2} \begin{pmatrix} (u+c)+(1-y)^2(\bar{d}+\bar{s}) \\ (d+s)+(1-y)^2(\bar{u}+\bar{c}) \\ 0 \\ 0 \end{pmatrix}$$

For neutral current reactions the situation is different. The photon is blind to the helicity of the electron but the Z^0 gives different contribution to e_L and e_R scattering as shown in sect. 3.1. Figure 12 shows the difference between the cross sections for $e_{L,R}^-$ and $e_{L,R}^+$ scattering. They amount to $\sim 60\%$ at Q^2 values of 10^4 GeV^2.

4. Production Of New Particles

4.1 Pair Production of Heavy Quarks

Photon-gluon fusion (Fig. 4) will be a strong source of heavy quarks. A discussion of the process can be found in Ref. 12. The total cross section depends on the quark mass approximately as

$$\sigma(eq \to Q\bar{Q}X) \sim M_Q^{-4}$$

Given a t quark mass of 40 GeV and a luminosity of $200 pb^{-1}$ the expected number of $t\bar{t}$ events is a few hundred. Top - like quarks can be searched for up to masses of 100 - 120 GeV.

The heavy quarks will essentially be photo produced ($Q^2 \approx 0$) and will be emitted in the direction of the incoming proton. Given the high mass these heavy quarks will decay into many particles ($\sim 20 - 25$ for $m_t = 40$ GeV) which are isotropically distributed in the plane perpendicular to the beams. Thus, the production of new

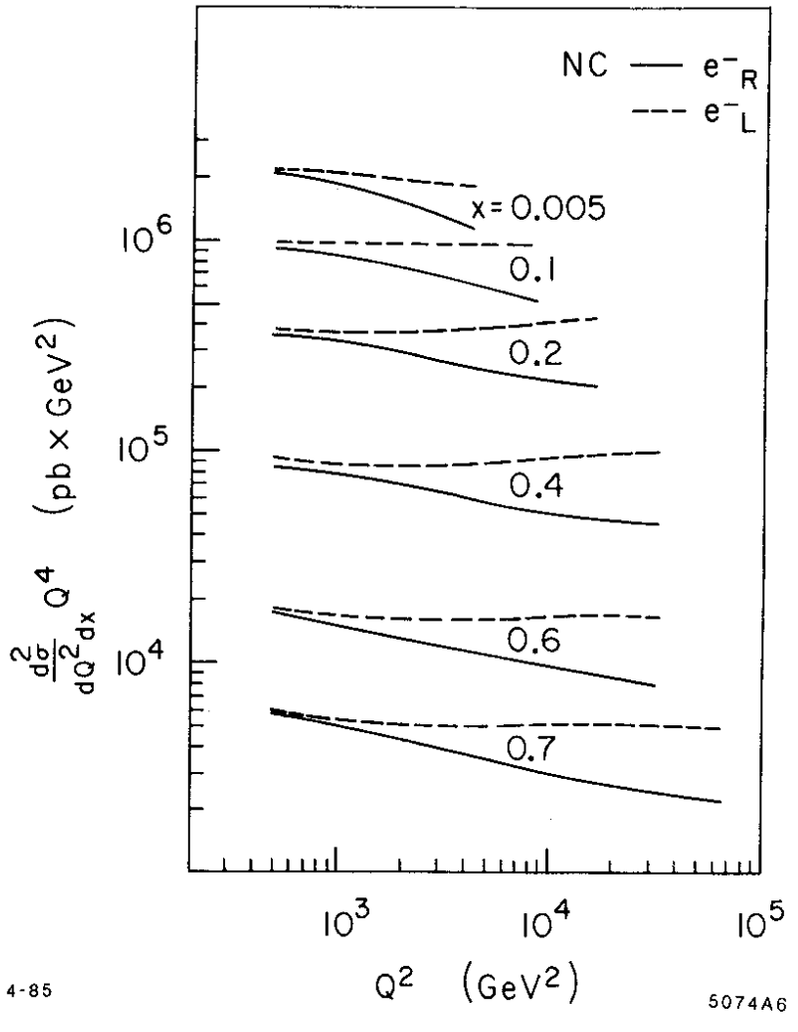

Figure 12. The neutral current cross section for left and right handed e^-

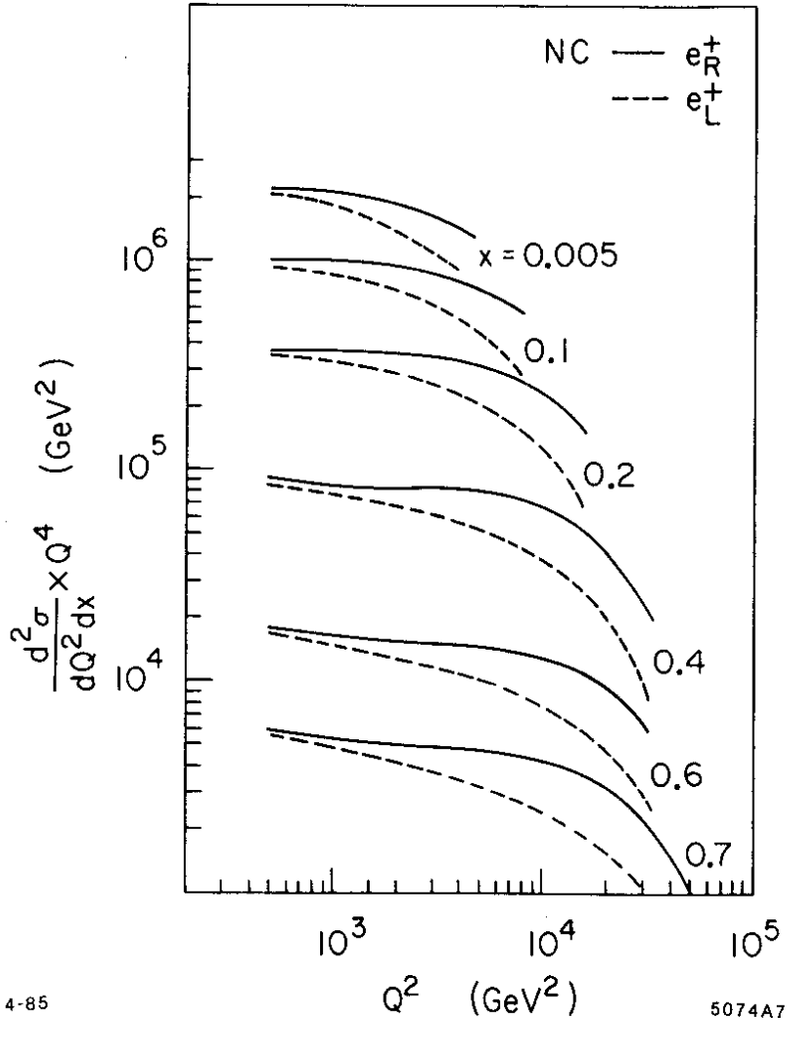

Figure 12. The neutral current cross section for left and right handed e^+.

heavy quarks should also be discernible from other processes. Figure 13 shows for illustration the production of a $t\bar{t}$ pair assuming $M_t = 40$ GeV.

Another possible source of Q production might be an intrinsic $Q\bar{Q}$ component in the nucleon. It has been argued for instance[13] that the $c\bar{c}$ component could be as large as 1% and could become an important contributor once Q^2 exceeds $\sim 4M_c^2$.

4.2 Vector Boson Production

Z^0 and $W^\pm$ production is expected to proceed predominantly through the diagrams shown in Fig. 14. The total cross sections are predicted to be[14]

$$\sigma(ep \to Z^0 X) \approx 0.1\, pb$$

$$\sigma(ep \to W^\pm X) \approx 0.05\, pb$$

leading to ~ 20 Z^0 events and ~ 10 $W^\pm$ events for 200 pb^{-1}.

In the (unlikely) case that Z^0 and $W^\pm$ have also a strongly interacting component the time honoured pomeron exchange (Figs. 15) may add to their production rate.

4.3 Higgs Production

Possible diagrams for production of Higgs particles are shown in Fig. 16. For a total of 200 pb^{-1} the expected yield of Higgs produced is not overwhelming:[15]

M_H =	10	20	50	100 *GeV*
number of events =	10	10	10	3

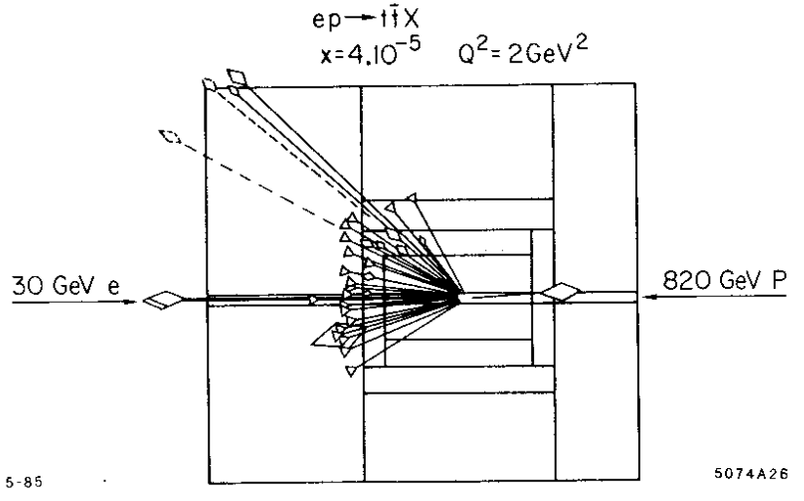

Figure 13. Example of a $t\bar{t}$ production event.

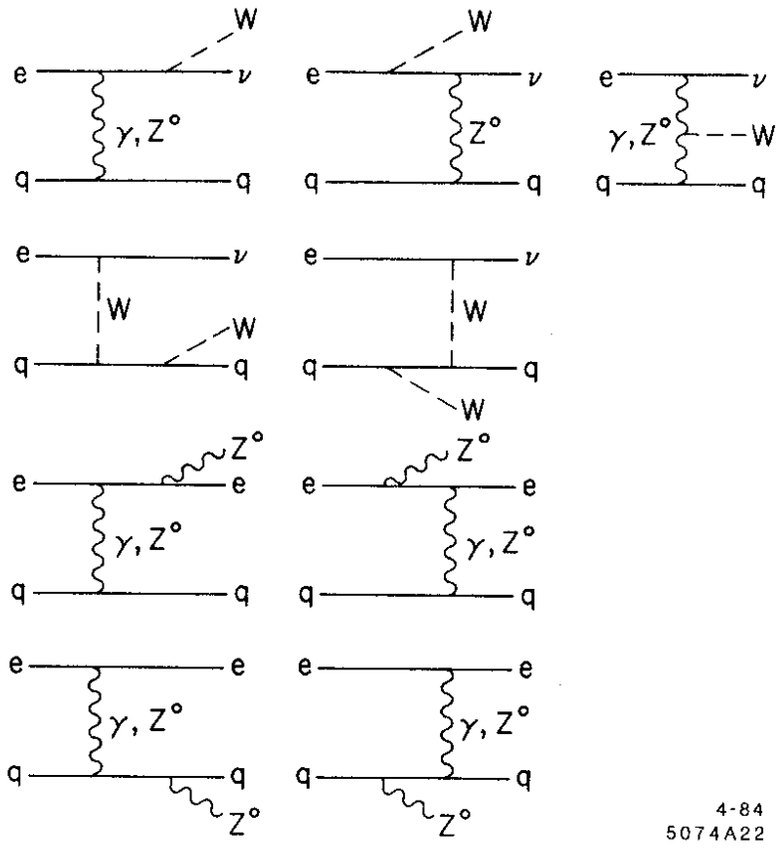

Figure 14. Diagrams for Z^0 and $W^{\pm}$ production.

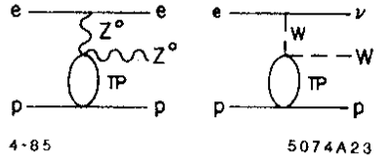

Figure 15. Diagrams for $Z^0, W^{\pm}$ production by pomeron exchange.

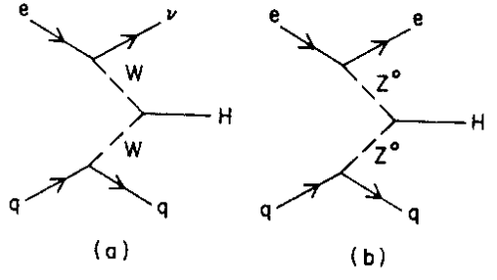

Figure 16. Diagrams for Higgs production.

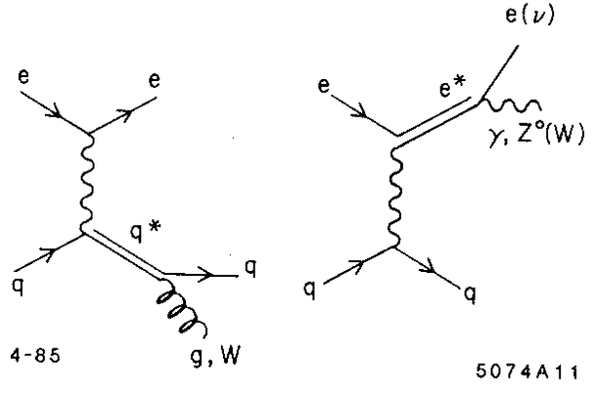

Figure 17. Diagrams for the production of excited quarks and leptons.

4.4 Excited Quarks and Leptons

If quarks and leptons are composites the existence of excited quarks and leptons q^*, e^* appears to be natural (remember p, Δ). Their production would follow the diagrams of Fig. 17. The production rates are sufficient to search for q^*, e^* up to masses of 250 GeV.[16]

4.5 New Currents, Quarks, Leptons

Suppose there exist new currents $X^0, X^\pm$ which link the known quarks and leptons to new quarks $Q = U, D, S, C, B, T$ and leptons L, and with coupling strengths equal to that of the standard weak interactions. The cross section for the dominant associated production of D and L^0 as depicted in Fig. 18 is given by

$$\frac{d\sigma}{dxdy} = \frac{G_F s}{2}\left(\frac{m_W}{m_X}\right)^4 \frac{1}{(1+\frac{sxy}{M_X^2})}$$

$$\left\{ xq(x)\left(1-\frac{m_L^2+m_D^2}{sx}\right) + x\bar{q}(x)\left(1-y-\frac{m_L^2}{sx}\right)\left(1-y-\frac{m_D^2}{sx}\right)\right\}$$

where

$$q(x) = u(x) + c(x) + \ldots$$

$$\bar{q}(x) = \bar{d}(x) + \bar{s}(x) + \ldots$$

The kinematically allowed regions for x and y are

$$\frac{(m_L+m_D)^2}{s} < x < 1$$

$$y_- < y < y_+$$

$$y_\pm = \frac{1}{2sx}\left[sx - m_D^2 - m_L^2 \pm \sqrt{(sx-m_D^2-m_L^2)^2 - 4m_D^2 m_L^2}\right]$$

The process will lead to the event rates shown in Fig. 19 as a function of m_D for different lepton masses m_L (assuming $m_z = 83$ GeV and 10 days of running at $L = 10^{31}\ cm^{-2}s^{-1}$); 200 pb^{-1} would probe up to $m_L + m_D \approx 220$ GeV.

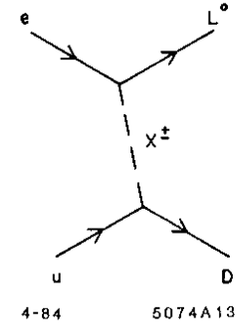

Figure 18. Diagram for new quark and lepton production.

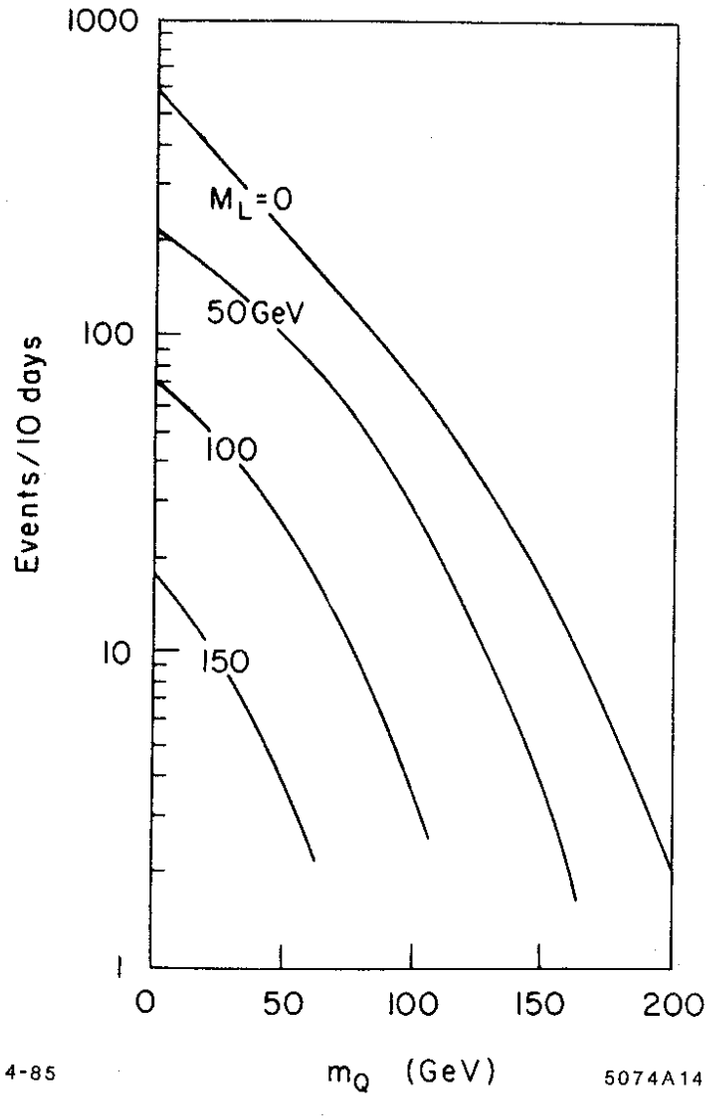

Figure 19. Production rates for $e^- p \to DL^0 X$.

4.6 Leptoquarks

Technicolour offers an alternative though not undisputed explanation for the Higgs mechanism. In this theory the Higgs is a pion-like composite: a state where a new quark and antiquark are bound together by the super strong technicolour force. Besides new quarks $U, D, \ldots$ new leptons $E, M, \ldots$ are also predicted which together lead to a new universe of particles. What is most exciting for HERA is the occurrence of leptoquarks $TLQ \equiv \bar{u}E, \ldots$ The expected mass hierarchy is as follows:

	mass
— technipions $(U\bar{D}, \ldots)$	0 (10 GeV)
— leptoquarks $(U\bar{E}, \ldots)$	0 (160 GeV)
— technicolour Octets $(U\bar{D}, \ldots)$	0 (240 GeV)

Leptoquarks would be within the reach of HERA experiments. The diagrams expected to dominate the production are given in Fig. 20. The cross section for $ep \to TLQ\,X$ is shown in Fig. 21 as calculated by.[17] Here θ_{et} is the mixing angle. Given a $\sin^2 \theta_{et}$ of ~ 0.05 leptoquarks with masses up to 180 GeV can be studied at HERA (Fig. 21).

Technicolour theories already have difficulties explaining the small $K_L^0 \to \mu^+\mu^-$ branching ratio, and no evidence has been found at PETRA or PEP for low-lying technipions.

4.7 Supersymmetric Particles

HERA is a hunter's paradise for supersymmetric particles–if they exist in the accessible mass range. The prototype reaction is associated production of squark $(\tilde{q})$ and slepton $(\tilde{\ell})$ by photino $(\tilde{\gamma})$, zino $(\tilde{Z})$ or wino $(\tilde{W})$ exchange, (Fig. 22). The cross section has been calculated in Ref. 18. Figure 23 shows the cross section as a function of the squark mass for different slepton mass values. If we demand at least 10 events per 200 pb^{-1} then squark plus slepton production can be studied up to mass values of $m_{\tilde{q}} + m_{\tilde{e}} = 160$ GeV.

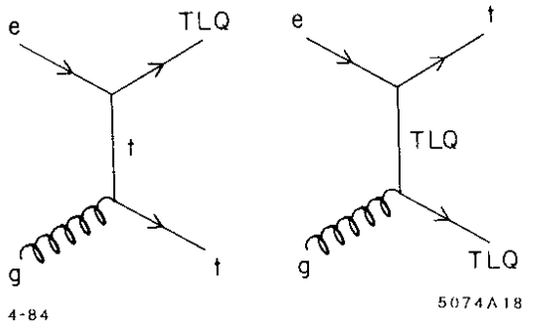

Figure 20. Diagrams for the production of leptoquarks.

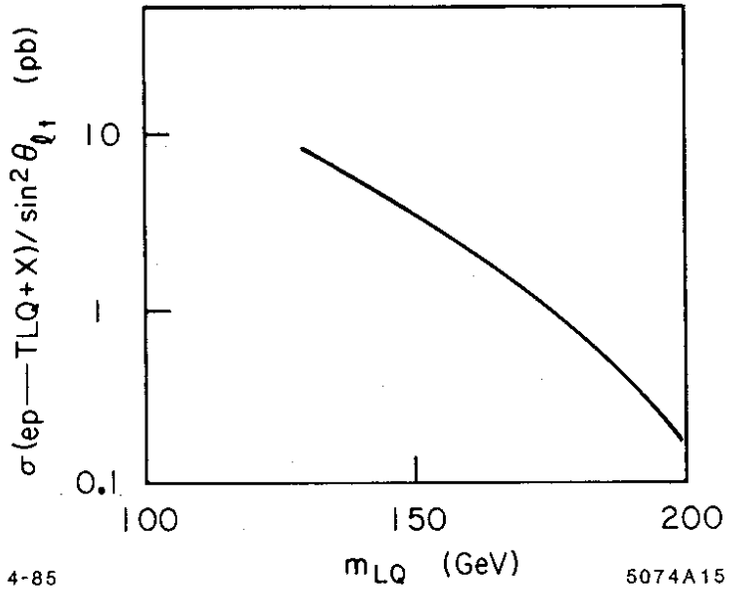

Figure 21. Cross section for the production of leptoquarks.

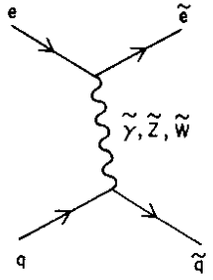

Figure 22. Diagram for $eq \rightarrow \tilde{e}\tilde{q}$.

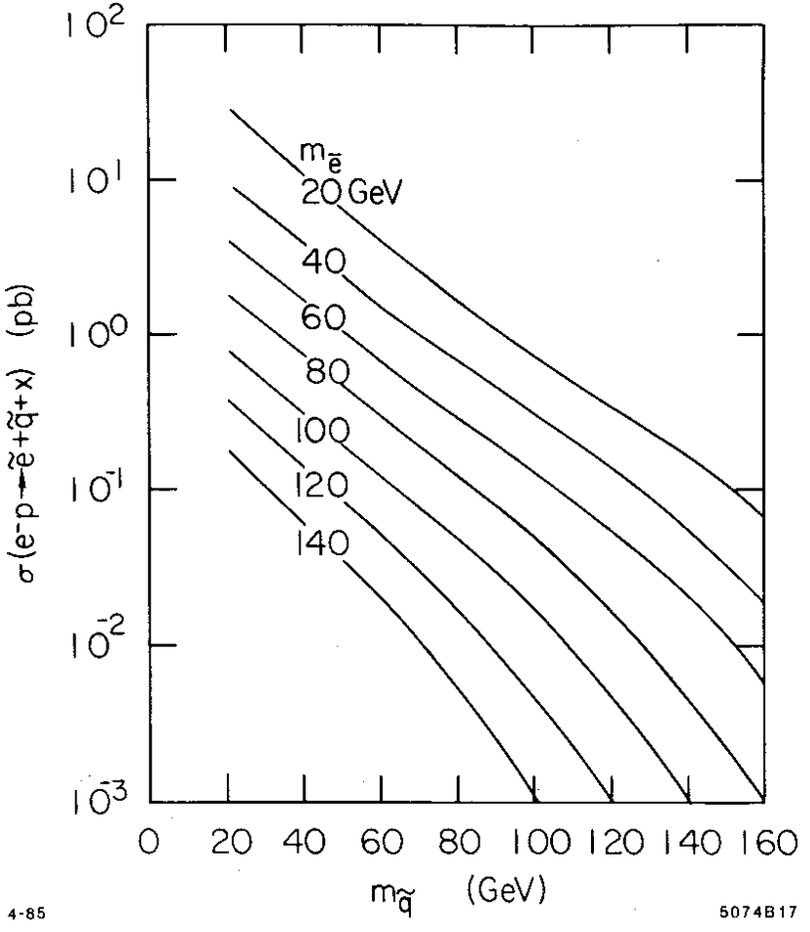

Figure 23. Cross section for the production of supersymmetric quarks and leptons.

The production of scalar leptons has been studied in Ref. 14. The dependence on the $e^{\pm}$ polarization has been analyzed in Ref. 19.

5. Detection Of New Processes

The mass range that is accessible to HERA for new particles was estimated in the previous sections by requiring the production of at least a few tens of these events a year. Since the yield of standard neutral and charged current events is many orders of magnitude larger one might wonder whether those few exotic events will be discernible from the ordinary processes – or whether their detection will be as difficult as e.g. that of the top quark at the $S\bar{p}pS$ collider.

The events should be visible if the dominating background is ordinary neutral current scattering ($eq \to eq$). This is a consequence of two facts: the kinematics in $eq \to eq$ is well defined, and, the decay of a new heavy object will spread the emerging quark (lepton) over a large volume in phase space. For definiteness consider the supersymmetric reaction discussed before,

$$eq \to \tilde{e}\,\tilde{q}$$

The event rate relative to the standard neutral current reaction, $eq \to eq$, is

$$\text{for } M_{\tilde{q}} + M_{\tilde{e}} = \begin{cases} 80\ GeV \\ 180\ GeV \end{cases} \quad \frac{\sigma(\tilde{e}\,\tilde{q})}{\sigma(eq)} \approx \begin{cases} 10^{-3} \\ 10^{-5} \end{cases}$$

The expected decay chains for $\tilde{q}$ and $\tilde{e}$ are

$$\tilde{q} \to q + \tilde{\gamma}$$

and

$$\tilde{q} \to q + \tilde{g} \to qg\tilde{G}$$

and

$$\tilde{e} \to e + \tilde{\gamma} \quad \text{or} \quad \tilde{e} \to e + \tilde{G}\ .$$

Under the assumption that $\tilde{\gamma}$ and $\tilde{G}$ are weakly interacting and leave the experiment

undetected the final state consists of an electron and a quark jet as in the case of an ordinary neutral current event. The difference lies in the kinematics as seen in the plane perpendicular to the beams. This is illustrated in Fig. 24.

In the standard case the electron and the quark jet are anticollinear and balance each other in transverse momentum. For the supersymetric process e and q are neither anticollinear nor do they balance each other in transverse momentum. These two facts can be used to suppress the background. How efficiently that suppression can be done is demonstrated in Fig. 25. Here the acollinearity angle $\Delta\varphi$ is plotted versus Δy which measures the difference in y values computed from the current jet and the scattered electron:

$$\Delta y = y_q - y_e$$

$$y_q = \frac{\Sigma E_i - P_{ti}}{2E_e}$$

$$y_e = 1 - \frac{E'_e - P'_{te}}{2E_e}$$

E_i, P_{ti} are the energies and longitudinal momentum components of the current jet particles; E'_e, p'_{t} are the energy and longitudinal momentum component (measured *w.r.t.* the incoming proton direction) of the scattered electron.

The distributions shown in Fig. 25 have been computed by a Monte Carlo technique for a reasonably realistic detector assuming a finite hadronic energy resolution ($\Delta E/E = 60\%/\sqrt{E}$) and a blind angular region around the beam pipe. Fig. 25(c) shows the result for $\sim 10^4$ standard neutral current events. As expected, the events cluster near $\Delta\varphi = \Delta y = 0$. In contrast, for the supersymmetric process (shown in Fig. 25(a) for $m_{\tilde{q}} = m_{\tilde{e}} = 40$ GeV and in Fig. 25(b) for $m_{\tilde{q}} = m_{\tilde{e}} = 100$ GeV) the events are spread all over the $\Delta\varphi, \Delta y$ map. Thus, supersymmetric events can be well isolated from the standard ones without significant loss in efficiency.

6. Summary And Conclusions

Structure functions of neutral and charged current reactions can be studied with

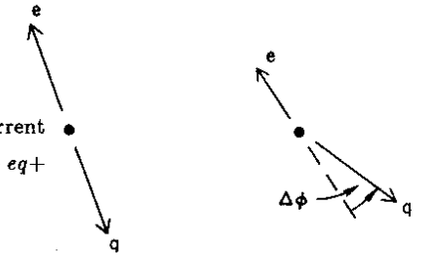

Figure 24. Comparison of the kinematics for the stand neutral current process, $eq \to eq$, and for the supersymmetric process $eq \to \tilde{e}\tilde{q} \to eq+$ missing particles.

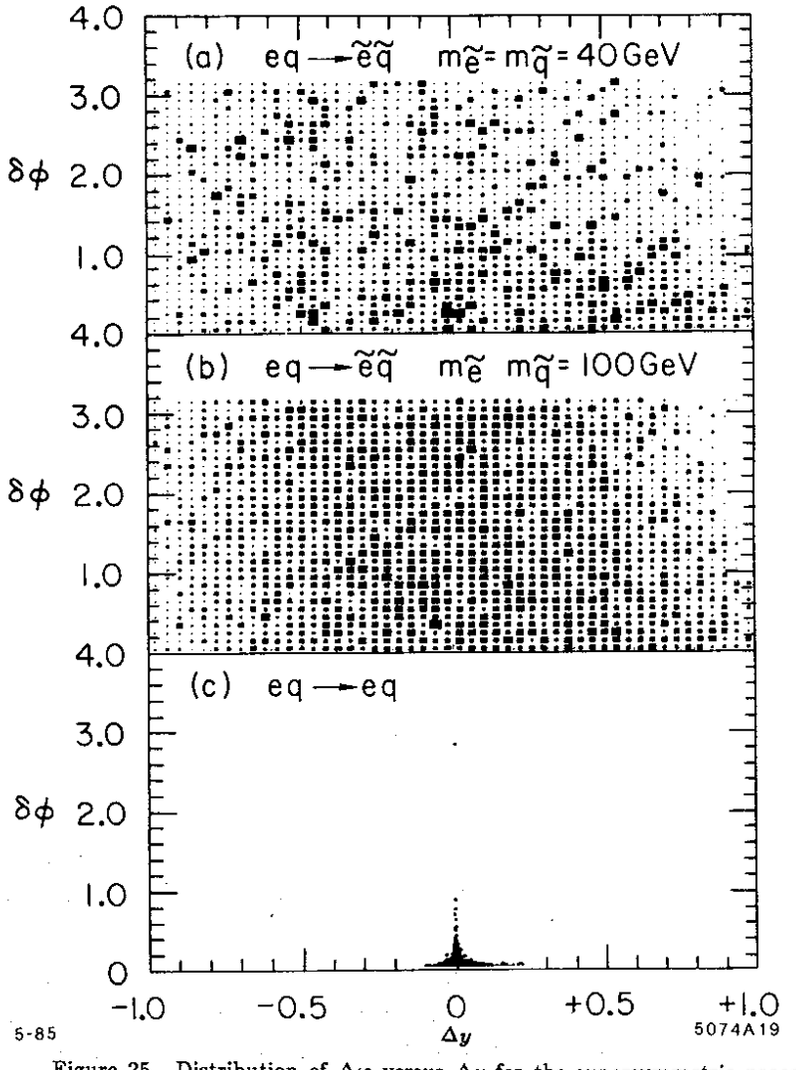

Figure 25. Distribution of $\Delta\varphi$ versus Δy for the supersymmetric process $eq \to \tilde{e}\tilde{q}$ with $m_{\tilde{e}} = m_{\tilde{q}} = 40$ GeV (a) and $m_{\tilde{e}} = m_{\tilde{q}} = 100$ GeV (b) and for the standard process $eq \to eq$ (c).

HERA for Q^2 values up to 30,000 – 40,000 GeV^2. The $Q^2 - \nu$ space will be extended by two orders of magnitude in either variable over what can presently be reached. Precise structure function values will provide a stringent test of QCD, will probe for substructure of quarks and leptons down to distances of $3.10^{-18}cm$, and could detect new neutral or charged pieces of the current. In the search for right handed weak currents longitudinally polarized electrons will be extremely useful.

HERA is potentially a rich source of new particles. Basically any state that has electric and/or weak charge can be produced up to masses of 200 - 250 GeV. The sensitivity in mass is shown in Table 3.

Table 3. Expected sensitivity in mass.

new W	800 Gev
new Z^0	800 GeV
right handed W	500 GeV
new quark (t like)	120 GeV
excited q^*, e^*	250 GeV
new quarks, leptons	220 GeV
leptoquarks	180 GeV
supersymmetric quark plus lepton	160 GeV

In many aspects HERA is complementary to LEP. It probes primarily the space like region and gives access to *charged* currents over a unique kinematic range. For a number of the newly proposed particles the mass range open to HERA experiments exceeds that of LEP II.

The design of an optimal detector for HERA poses a veritable challenge. The large momentum imbalance between incident electron and proton and the nature of space like processes throw most final state particles into a narrow cone around

the proton direction. On the other hand, the standard neutral current reaction in HERA, $ep \to eX$, offers an important advantage over $\bar{p}p/pp$ interactions. By tagging the scattered electron the kinematics of the relevant subsystem is determined. It is this handle which provides HERA experiments with a special sensitivity to new exotic particles.

Acknowledgments: I am very grateful to Profs. R. Peccei, P. Soding and R. Taylor for a critical reading of the manuscript.

References

1. B. H. Wiik, Electron - Proton Colliding Beams, the Physics Programme and the Machine, proc. 10th SLAC Summer Institute, ed. A. Mosher, 1982 p.233. DESY International Report, DESY F35-83-01 (1983).

   Proc. 1984 ICFA Seminar on Future Perspectives in High Energy Physics, May 14-20, 1984, KEK, Japan, eds. S. Ozaki, S. Kurokawa, Y. Unno, p.23.

2. C. H. Llewellyn-Smith and B.H. Wiik, DESY Report 77/36 (1977).

3. Proc. Study of an *ep* facility for Europe, ed. U. Amaldi, DESY Report 79/48 (1979);

   HERA, proposal report DESY-HERA 81/10, (1981).

   Résumé Discussion Meeting "Physics with *ep* Colliders in view of HERA " Wuppertal, report DESY-HERA 81/18, (1981);

   Proc. Workshop "Experimentation at HERA ", NIKHEF, Amsterdam, June 9 - 11, 1983, report DESY-HERA 83/20, (1983);

   Proc. Discussion Meeting on "HERA Experiments", Genova, Oct. 1 - 3, 1984 report DESY-HERA 85/01, (1985).

   G. Altarelli, B. Mele and R. Rückl CERN Report TH3932, (1984).

   J. A. Bagger, M.E. Peskin, SLAC-PUB-3447 (1984).

   R. J. Cashmore *et al.*, "Exotic Phenomena in High Energy *ep* Collisions," Physics Reports (1985).

4. See *e.g.* E. Lohrmann, K.H. Mess, DESY-HERA 83/08 (1983).

5. M. Glück, H. Hoffmann, E. Reya, Z. Phys. C13 119, (1982).

6. E. J. Eichten, K.D. Lane, M.E. Peskin, Phys. Rev. Lett. 50 811, (1983);

   Also see R. Rückl, Phys. Lett. 129B 363, (1983).

7. MAC Collaboration, E.Fernandez *et al.*, Phys. Rev. Lett. 50 123,(1983); TASSO Collaboration, M. Althoff *et al.*, Z. Phys. 22 13, (1984) Phys. Lett.

138B 441, (1984); MARK J Collaboration, B. Adeva *et al.*, Phys. Rep. 109 131, (1984); HRS Collaboration, D. Bender *et al.*, ANL-HEP-PR-03,71; PLUTO Collaboration, Ch. Berger *et al.*, Z. Phys. 27 341, (1985).

8. I. Bars, M. J. Bowick, K. Freese, Phys. Lett. 138B 159, (1984).

9. c.f. J.C. Pati, A. Salam, Phys. Rev. D. 10 275, (1974); R. N. Mohapatra, J. C. Pati, *ibid*, 566, 2559 (1975). R. N. Mohapatra, R. E. Marshak, Phys. Rev. Lett. 44 1316, (1980).

10. R. N. Mohapatra, G. Senjanovic, Phys. Rev. Lett. 44 912, (1980).

11. G. Senjanovic, Proc. SSC Fixed Target Workshop, The Woodlands, Tx, 1984. D. P. Stoker *et al.*, LBL - 18935 (1985) and Phys. Rev. Lett.

12. J. P. Leveille, T. Weiler, Nucl. Phys. B147 147, (1979).

13. S. J. Brodsky, J. F. Gunion, SLAC-PUB-3527 (1984).

14. G. Altarelli, G. Martinelli, B. Mele, R. Rückl, CERN TH 4094, (1985).

15. J. Ellis, M. K. Gaillard, D.V. Nanopoulos, Nucl. Phys. B106 292, (1976).

16. See e.g. J. H. Kühn, H. D. Tholl, P. M. Zerwas, CERN TH 4131, (1985).

17. S. Rudaz, J. A. M. Vermaseren, CERN TH 2961 (1981).

18. S. K. Jones, C. H. Llewellyn-Smith, Nucl. Phys. B217 145, (1983).

19. D. P. Harrison, Nucl. Phys. B249 704, (1985). L. Marlean, SLAC-PUB-3533 (1984).